Computers and Fluids 263 (2023) 105958

Contents lists available at ScienceDirect

Computers and Fluids

journal homepage: www.elsevier.com/locate/compfluid

On the flow of soft suspensions through orifices

Linlin Fei [a,*], Andrea Puglisi [b,c], Sauro Succi [d,e], Kai H. Luo [f]

[a] Chair of Building Physics, Department of Mechanical and Process Engineering, ETH Zürich (Swiss Federal Institute of Technology in Zürich), Zürich 8092, Switzerland
[b] Istituto dei Sistemi Complessi, CNR and Dipartimento di Fisica, Università di Roma Sapienza, Piazzale Aldo Moro 2, 00185 Rome, Italy
[c] INFN, University of Rome Tor Vergata, Via della Ricerca Scientifica 1, 00133 Rome, Italy
[d] Center for Life Nano Science at La Sapienza, Istituto Italiano di Tecnologia, 295 Viale Regina Elena, I/00161 Roma, Italy
[e] Harvard Institute for Applied Computational Science, Cambridge, MA 02138, USA
[f] Department of Mechanical Engineering, University College London, Torrington Place, London WC1E 7JE, UK

ARTICLE INFO

MSC:
00-01
99-00

Keywords:
Soft suspensions
Lattice Boltzmann simulations

ABSTRACT

The behavior of confined suspensions of soft droplets under pressure-driven flow, passing an obstacle within a planar channel, is investigated by means of a mesoscopic lattice Boltzmann model capable of simulating soft non-coalescing droplets. The simulations reveal that the threshold of the pore size, below which the flux vanishes, is between 1 and 2 droplet diameters, and increases with the packing fraction. Moreover, we show that the classical Beverloo relation between the total flux and the pore size is not suitable for the soft suspensions considered here.

1. Introduction

The flow of particle suspensions is of widespread practical [1,2] and fundamental [3–5] interest. Hard particle suspensions or granular media are the subject of a decades-long activity in the realm of statistical mechanics and kinetic theory [6,7]. On the contrary, dense and soft flowing suspension systems are widespread in engineer and applied research [8]. They also draw the interest of experimental physicists [9–11], but elude the effort of theorists and for this reason lack a systematic and comprehensive theoretical framework.

One challenge of understanding and controlling the suspension rheology is that the response is nonlinear, with a forcing threshold below which the medium is static [12–15]. Furthermore, just above threshold the response may be intermittent even though the forcing is steady. Familiar examples include avalanches down the surface of a heap as well as gravity-driven discharge from a horizontal hole at the bottom of a deep container or "silo". For the latter, the mass discharged per unit time is given by the "Beverloo" relation:

$$W = C\rho_b (g D_c)^{1/2} D_c^2 \left(\frac{D - D_c}{D_c}\right)^{n-1/2} \tag{1}$$

where n is spatial dimensionality, ρ_b is the density of the hard particle suspensions, $g = 980\ \mathrm{cm/s^2}$, D is the hole diameter, $D_c = k_c d$ is the critical diameter (with d the grain diameter) below which average flow disappears, and C and k_c are dimensionless fitting parameters [16]. Accordingly, and in contrast with viscous fluids, the discharge of grains is independent of filling depth. Typical ranges for the numerical constants are $0.5 < C < 0.7$ and $1.2 < k_c < 3$, depending on grain shape and friction. The Beverloo equation entails the existence of a threshold hole diameter, D_c, of a few grains across, below which the flux vanishes. Just above this cutoff, the flow is intermittent with random jamming events [17,18].

Jamming through an orifice is highly useful for probing the extreme limits of flowing particle suspensions, since in this situation the bulk – continuum-like – behavior of a large system may be influenced by a relatively small number of particles near the hole. Furthermore, jamming is a natural phenomenon that illustrates spontaneous evolution from a freely flowing state to a jammed state with no change in the external forcing. Similar issues are important for understanding the flow of suspensions and emulsions [19–26] through constrictions, where the hydrodynamics of the flowing fluid as well as the capillary effects must be taken into account, e.g., the flow of vortices through an array of pinning sites in superconductors [27], as well as automotive [28] and pedestrian [29] traffic. In spite of many simulations [17,30] and experiments in both two- and three-dimensional hoppers [12,18,31,32], the ability to predict or control clogging is still lacking [33].

The flow of suspensions through porous structures, which leads to a partial or full filtration, is widely used in industry either to purify fluids or to separate species in chromatography, microfluidics, or nanofluidics [34]. Filtration has also a major impact in the environment (water and wastewater treatment, drilling well productivity, pollutant

* Corresponding author.
E-mail address: linfei@ethz.ch (L. Fei).

https://doi.org/10.1016/j.compfluid.2023.105958
Received 30 January 2023; Received in revised form 6 April 2023; Accepted 19 May 2023
Available online 9 June 2023

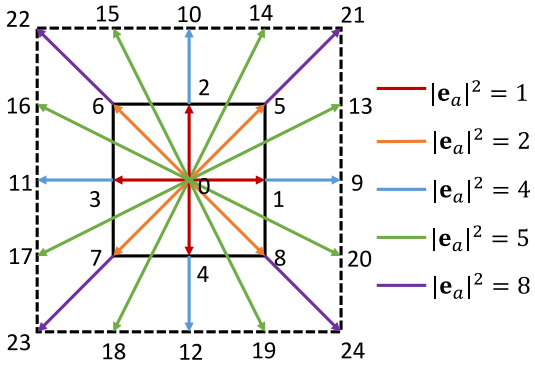

Fig. 1. The discrete lattice used in this work. The fluid lives in the D2Q9 lattice while the interactions extend to the D2Q25 lattice.

storage in soils, unbalance of ecosystems or floods due to accumulation of fine sediments in gravel-bed streams, etc.) [35–37] A straightforward application of understanding obstruction of suspensions is found in ecological engineering: there, an alternative that is becoming widely used for removing pollutants from waste water is the use of subsurface flow treatment. The most important drawback of this technique is its unpredictable lifetime, mostly limited by clogs that obstruct the pores [38].

In this paper we offer a new insight in the flow behavior of soft suspensions, based on the mesoscopic lattice Boltzmann simulations of the soft suspensions under pressure-driven flow, passing through an obstacle within a planar channel. In Section 2, we give a brief introduction of the adopted numerical method. In Section 3, the simulation results are analyzed and discussed. Finally, a short summary is given in Section 4.

2. Numerical method

In this paper, a two-species mesoscopic lattice Boltzmann (LB) model based on an extended pseudopotential interactions [39,40] is adopted to investigate the flow behavior of soft suspensions. The LB model takes the form (see [41–44] for details):

$$f_{k,i}(\mathbf{x}+\mathbf{e}_i\Delta t, t+\Delta t) = f_{k,i} - \frac{\Delta t}{\tau_k}(f_{k,i} - f_{k,i}^{eq}) + \Delta t F_{k,i}. \tag{2}$$

where $f_{k,i}$ is the probability of finding a particle of species k ($k = 1, 2$) at the space $\mathbf{x}$ and time t, moving along the ith direction $\mathbf{e}_i$ of the two-dimensional nine-velocity (D2Q9) lattice in Fig. 1. $\Delta t = 1$ is the lattice time step. The right-hand side, computed at $(\mathbf{x}, t)$, is the time relation (due to collisional interactions) toward the local equilibrium $f_{k,i}^{eq}$ on a time scale τ_k. $F_{k,i}$ is a forcing term representing the effects of the total force $\mathbf{F}_k$ acting upon each species of the suspensions [45].

The total force imposed on each species is $\mathbf{F}_k = \mathbf{F}_k^b + \mathbf{F}_k^r + \mathbf{F}_k^c$, where $\mathbf{F}_k^b$ is the body force, $\mathbf{F}_k^r$ is interspecies repulsive force, acting between the two species, and $\mathbf{F}_k^c$ the intraspecies force, encoding the competition between a short range (within the first-belt D2Q9 lattice in Fig. 1) attraction and a mid-range (extending to the D2Q25 lattice in Fig. 1) repulsion within each species [39,40,46]. The repulsive interspecies force is defined as usual [39],

$$\mathbf{F}_k^r = -\rho_k(\mathbf{x})\sum_{\bar{k}} G_{k\bar{k}} \sum_{i=0}^{8} w(|\mathbf{e}_i|^2)\rho_{\bar{k}}(\mathbf{x}+\mathbf{e}_i\Delta t)\mathbf{e}_i, \tag{3}$$

where $G_{k\bar{k}} = G_{\bar{k}k}$ is the strength coefficients for the interspecies interaction, and the weights are $w(0) = 4/9$, $w(1) = 1/9$, and $w(2) = 1/36$. The competing interaction force is explicitly written as [46],

$$\mathbf{F}_k^c = -G_{k,1}\psi_k(\mathbf{x})\sum_{i=0}^{8} w(|\mathbf{e}_i|^2)\psi_k(\mathbf{x}+\mathbf{e}_i\Delta t)\mathbf{e}_i$$
$$- G_{k,2}\psi_k(\mathbf{x})\sum_{j=0}^{24} p(|\mathbf{e}_j|^2)\psi_k(\mathbf{x}+\mathbf{e}_j\Delta t)\mathbf{e}_j, \tag{4}$$

where $G_{k,1}$ and $G_{k,2}$ are the strength coefficients for the short-range and middle-range interactions respectively, and the weights for D2Q25 lattice are $p(0) = 247/420$, $p(1) = 4/63$, $p(2) = 4/135$, $p(4) = 1/180$, $p(5) = 2/945$ and $p(8) = 1/15120$. The pseudopotential originally suggested by SC [39,40], $\psi_k(\rho_k) = \rho_0(1 - e^{-\rho_k/\rho_0})$ (with a uniform reference density $\rho_0 = 1.0$ for each component) is adopted. The above definition of $\mathbf{F}_k^c$ is to mimic the spatially complex (non-monotonic) interactions among molecules within each species. We wish to point out that the incorporation of $\mathbf{F}_k^c$ provides an important extension of the original pseudo-potential model [39,40], as it allows the emergence of supramolecular forces, e.g., positive disjoining pressure [47], in the lattice kinetic model. Such an extension has met with significant success in reproducing many features of a variety of soft flowing systems, such as aging, elastoplastic rheology, and structural frustration, in confined and unbounded flows of micro-emulsions [47–49]. More details about the numerical scheme adopted in this paper can be found in [45].

We prepare the soft suspensions by packing monodisperse droplets in a 2D pressure-driven flow, within a micro-channel of size $3L = 990$ and $L = 330$ along the streamwise (x) and cross-flow (y) directions, respectively. Moreover, an obstacle with height H is placed along the y direction at $x = L$. The no-slip boundary conditions for the velocity are imposed on the top and bottom walls, as well as the obstacle; non-wetting boundary conditions (contact angle of $\theta = 180°$) are applied for the droplets. For the droplet (surrounding fluid) occupied region, the species densities are approximately $\rho_1 = 0.02, \rho_2 = 1.0$ ($\rho_1 = 1.0, \rho_2 = 0.02$), with unity dynamics viscosity ratio $\mu_1 = \mu_2 = 0.1$. The mass packing fractions Φ are tuned within $0.412 \le \Phi \le 0.622$ via changing the numbers of the equal-size droplets, with diameter $d = 30$. The pressure difference Δp is set to give a peak velocity $U_0 = 0.05$ for the corresponding single-species Poiseuille flow, and imposed via a homogeneous body force $\Delta p/3L$. Therefore, the pressure boundary condition at the inlet and outlet of the channel is replaced by the periodic condition. In the paper, the interspecies force $\mathbf{F}_k^r$ is tuned to realize a surface tension $\gamma = 0.02$ by setting $G_{k\bar{k}} = G_{\bar{k}k} = 2.33$, and the competing interaction force $\mathbf{F}_k^c$ is tuned with $G_{k,1} = -10$, and $G_{k,2} = 8$ to achieve a positive disjoining pressure, sufficient to avoid droplet coalescence. The propensity of the droplet to deform under shear, is usually measured by the Weber number $We = \rho d u^2/\gamma$, which in our case is well below 0.1. We note that the LB units are used for convenience, while the appropriate mapping between LB units and physical units can be found in [50,51].

3. Results

In our simulations, the obstacle size is changed progressively to study the effect of the (dimensionless) pore size $\delta = D/d$, with $D = (L-H)/2$ the real pore size, on the flowing behavior of the suspensions. A typical snapshot for $\delta = 4.5$ at $\Phi = 0.622$ is shown in Fig. 2. It is seen that our numerical method captures the main features of such suspensions, including stable and non-coalescing droplets, locally moderate deformations, and non-wetting boundary conditions for the droplets. We wish to point out that, without the obstacle, the present system reduces to the pressure-driven suspensions studied in our previous work [45], where our numerical scheme has been verified by empirical expressions [52] for the effective viscosity of the suspensions as a function Φ.

In Fig. 3, we show the horizontal average velocity u (normalized by U_0) as a function of y for different packing fractions at $\delta = 4.5$. Different from the Poiseuille flow profile (single-species, $\Phi = 0$), we see the velocity profile flattens gradually in the central region of the channel with the increase of Φ, as expected for such kind of non-Newtonian fluid [45,47]. We note the characteristic velocity in our system is $u <$ 0.01. The corresponding Reynolds number (based on L and μ_1) is less

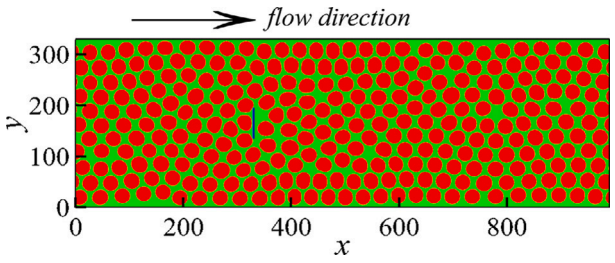

Fig. 2. A typical snapshot of pressure-driven soft suspensions in a planar channel at packing fraction $\Phi = 0.622$. The red and green color represents high and low density of droplets, respectively, and the obstacle is marked as the blue strip along y direction at $x = 330$. The obstacle height is $H = 60$, giving the pore size $\delta = 4.5$.

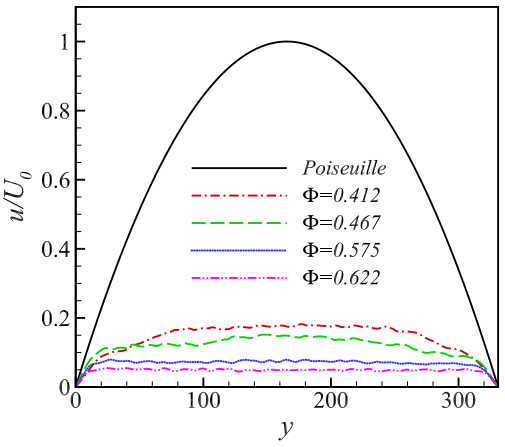

Fig. 3. Plot of the velocity profiles at different packing fractions Φ at $\delta = 4.5$.

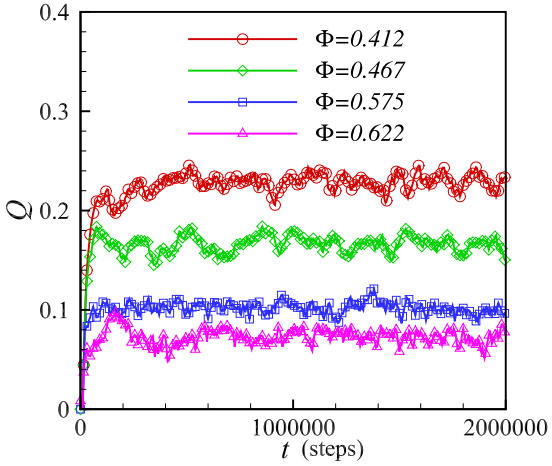

Fig. 4. Time evolution of the global flux of the system at different packing fractions.

than 33, out of the region of flow instability in single-species flow [41], i.e., periodically shed vortices.

To quantify the behavior of the suspensions, the global flux of the system is measured. In Fig. 4, the time evolution of the normalized flux,

$$Q = [\int_0^L u(y)dy]/(2U_0L/3), \tag{5}$$

is compared among different packing fractions. It is seen that the flux for each case increases to an approximately steady value, in spite of some fluctuations, after the first 2×10^5 steps. The average flux $\bar{Q}$ can then be obtained by the time average of Q in the steady stage. An interesting point is the relation between flux through the hole and peak

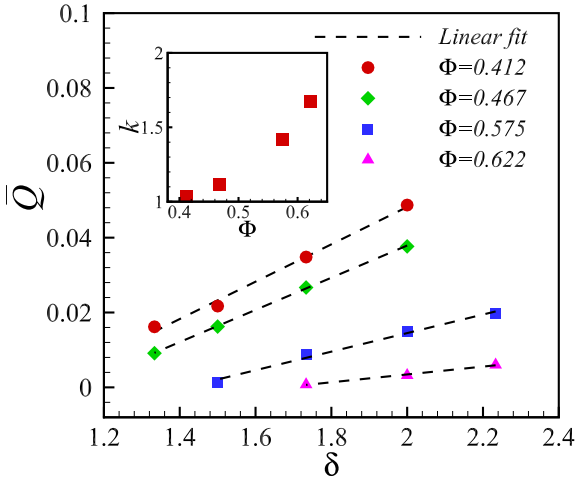

Fig. 5. Plot of global flowing flux as a function of the relative pore size $\delta = D/d$ near the zero-flux point ($\bar{Q} \to 0$). Through numerical extrapolation, we can obtain the horizontal intercept k, i.e., the zero point of $\bar{Q}$, for each case. Inset, plot of the horizontal intercept k as a function of Φ.

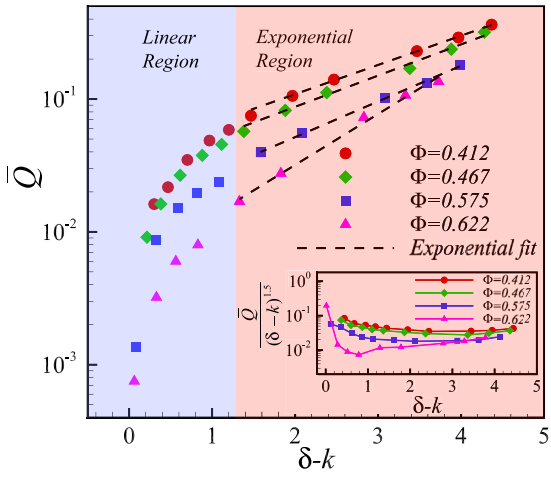

Fig. 6. Semi-log plot of the global flowing flux $\bar{Q}$ as a function of the relative pore size $\delta - k$, at different mass packing fractions. The phase diagram can be divided into a linear region and an exponential region, at the smaller and larger relative pore size, respectively. Inset, plot of the global flowing flux $\bar{Q}$ by $(\delta - k)^{3/2}$ as a function of $\delta - k$.

velocity U_0, which can be considered equivalent of the free fall velocity in hopper experiments [53,54]. Since $\bar{Q}$ is the flow velocity (averaged over the transverse direction L) normalized by the peak velocity U_0 itself, the real flux divided by density, $W/(\rho_1+\rho_2)$, is QU_0L, and this – at large enough D – should be compared to U_0D. In conclusion we should verify if $Q \sim D/L$. For instance in the region where $D \sim 10^2$ we observe $Q \sim 0.2$, which roughly agrees with the simple dimensional expectation. In order to see the robustness of this relation, we have also checked that fluxes W collapse when increasing L at constant forcing (not shown).

We now move to study the effect of pore size on the global flowing flux (or the permeability) of the system. Similar to the case in dry granular materials, it is important to evaluate the forcing threshold, below which the suspensions are fully jammed ($\bar{Q} = 0$). In the simulations, it is hard to directly obtain the pore size at which the flux $\bar{Q} = 0$ is exactly zero. Alternatively, the threshold value of δ can be obtained by finding the intercept of the function between $\bar{Q}$ and δ. Although the explicit relationship is unknown yet, it is reliable to find the intercept by linearly fitting the change of $\bar{Q}$ with δ near the zero-flux point, as shown in Fig. 5. In the inset, we show that the jammed pore size k is between 1.0 and 2.0 and increases with Φ. We note that

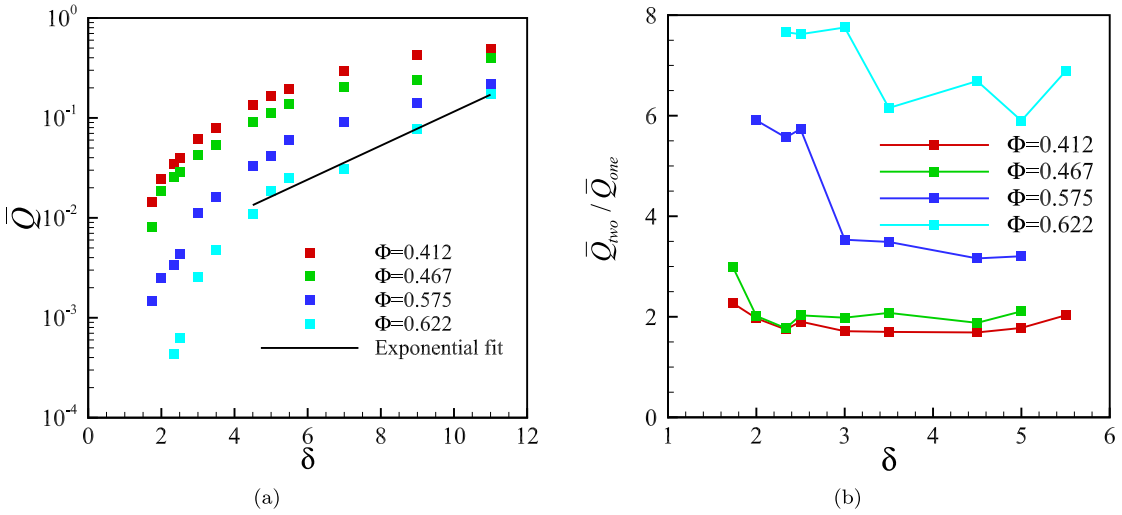

Fig. 7. Case of a single hole. (a): semi-log plot of the global flowing flux $\bar{Q}$ as a function of the relative pore size $\delta - k$, at different mass packing fractions. (b): ratio between flows with two and one holes as a function of δ for different packing fractions.

for dry granular matters, such a jammed pore size is usually around $1.2 \sim 3.0$ [16], and for dilute suspensions the smallest relative pore size for the penetration is convergent to $k = 0$ ($\Phi \to 0$), while our system is located in between. Studying the configuration of droplets in the jammed regime, we have seen that structures similar to static arches just before the holes appear.

Then, we consider to verify the applicability of the Beverloo relation in the present soft suspensions. Inspired by the Beverloo relation, we then consider the change of $\bar{Q}$ with $\delta - k$. As shown in Fig. 6, with the decrease of the $\delta - k$, it is more and more difficult to drive the "pass" of the droplets through the obstacle, namely producing a smaller $\bar{Q}$. For a given $\delta - k$, $\bar{Q}$ is also decreased with the increase of Φ, which is as expected and consistent with the case in planar channel without the obstacle [45]. For the present simulations, we find that our data are not in agreement with the Beverloo relation for dry granular materials. Mainly, we could not find a range where the 3/2 power-law between $\bar{Q}$ and $\delta - k$ can be convincingly fit: this is better seen in the inset where the rescaled flux does not show any tendency to be constant. Nevertheless, we find the semi-log of the plot shows a very good linear fit at large pore size, i.e., $\delta - k \geq 1$, indicating an exponential dependence of permeability on pore size in the region far from the threshold. When the pore size is further decreased, the measured flux $\bar{Q}$ deviates from the exponential law and linearly drops to zero, corresponding to the cases shown in Fig. 5.

For the sake of completeness we have considered two variants of the model. The first variation is going from two holes to a single hole, where the obstacle with an open hole in the middle is located at $x = L$. The main results are seen in Fig. 7. The phenomenology is similar, but the flow with one hole is much slower than half of the flow with two holes when the volume fraction is large, supposedly because of the growth of spatial correlation and therefore more and more relevant boundary effects.

The second variation consists in considering a bi-disperse system, obtained by preparing droplets with initially the same radius but different density: they rapidly deformate and tend to two populations with different radii (with a radius ratio of 1.2 : 1.0). The results for fluxes are shown in Fig. 8 and apparently bear no relevant differences with respect to the monodisperse case. This is important in order to evaluate the effect of disorder in the system.

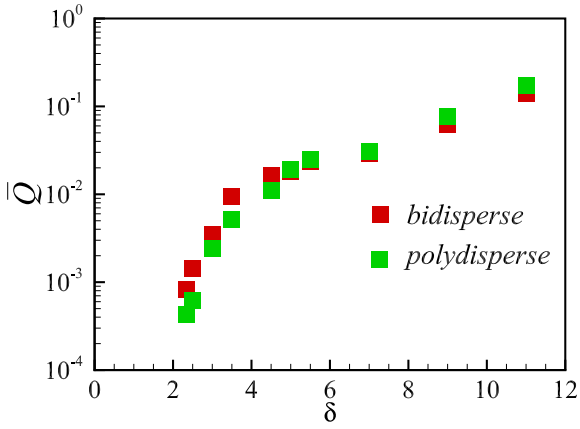

Fig. 8. Effect of bidispersity for the flux as a function of δ at $\Phi = 0.622$.

4. Conclusion

In summary, soft suspensions with equal-size droplets in a pressure-driven channel flow with an obstacle is simulated using a two-species mesoscopic lattice Boltzmann method. By changing the obstacle size, the behavior of soft suspensions in such geometry is numerically investigated. With increasing volume fraction of the dispersed phase (Φ), the velocity profile flattens in the channel center, deviating from the classical Poiseuille flow profile in the single component limit ($\Phi \to 0$). With decreasing pore size, the global flowing flux drops dramatically and the threshold pore size, below which the traverse of droplets fully disappear, i.e. (jamming), is obtained by linear interpolation near the zero-flux point.

Our numerical results show that the threshold of the dimensionless pore size, below which the flux vanishes, is between $k_c = 1.0$ and 2.0, and increases with Φ. Moreover, we find that the global flowing flux of the soft suspensions first exhibits an exponential dependence on the relative pore size, followed by a linear dependence, rather than the 3/2 power-law dependence as in the classical Beverloo relation for the hard particle suspensions. The phenomenological law holds for both two holes and single-hole systems and is also robust against slight loss of the monodispersity. In addition to the interests in statistics and soft matter physics, the present work provides new insights into many applications involving suspensions flow in confined space, for example, pedestrian dynamics [29], foam injection for enhanced oil recovery [55] and microfluidic scaffolds for tissue engineering [56], to name but a few.

Declaration of competing interest

The authors declare that they have no known competing financial interests or personal relationships that could have appeared to influence the work reported in this paper.

Data availability

Data will be made available on request.

Acknowledgments

The research leading to these results has received funding from the European Research Council under the European Union Horizon 2020 Framework Programme(No. FP/2014-2020)/ERC Grant Agreement No. 739964 (COPMAT). Supercomputing time on ARCHER is provided by the UK Consortium on Mesoscale Engineering Sciences (UKCOMES) under the UK Engineering and Physical Sciences Research Council Grant Nos. EP/R029598/1 and EP/T015233/1.

References

[1] Nedderman RM. Statics and kinematics of granular materials. NY: Cambridge University Press; 1992.
[2] Muzzio FJ, Shinbrot T, Glasser BJ. Powder technology in the pharmaceutical industry: The need to catch up fast. Powder Technol 2002;124:1.
[3] Jaeger HM, Nagel SR, Behringer R. Granular solids, liquids, and gases. Rev Modern Phys 1996;68(4):1259–73.
[4] Duran J. Sands, powders, and grains: An introduction to the physics of granular materials. NY: Springer; 2000.
[5] Jamming and rheology: Constrained dynamics on microscopic and macroscopic scales. NY: Taylor and Francis; 2001.
[6] Puglisi A. Transport and fluctuations in granular fluids. Springer; 2015.
[7] Brilliantov NV, Pöschel T. Kinetic theory of granular gases. Oxford: Oxford University Press; 2004.
[8] Coussot P. Rheometry of pastes, suspensions, and granular materials: Applications in industry and environment. John Wiley & Sons; 2005.
[9] Jop P, Forterre Y, Pouliquen O. A constitutive law for dense granular flows. Nature 2006;441:727.
[10] MiDi G. On dense granular flows. Eur Phys J E 2004;14:341.
[11] Forterre Y, Pouliquen O. Flows of dense granular media. Annu Rev Fluid Mech 2008;40:1.
[12] Sheldon HG, Durian DJ. Granular discharge and clogging for tilted hoppers. Granul Matter 2010;12:579.
[13] Tang J, Behringer RP. How granular materials jam in a hopper. Chaos 2011;21(4):041107.
[14] Mort P, Michaels J, Behringer R, Campbell C, Kondic L, Langroudi MK, et al. Dense granular flow—a collaborative study. Powder Technol 2015;284:571–84.
[15] Tang J, Behringer RP. Orientation, flow, and clogging in a two-dimensional hopper: Ellipses vs. disks. Europhys Lett 2016;114(3):34002.
[16] Beverloo WA, Leniger HA, van de Velde J. The flow of granular solids through orifices. Chem Eng Sci 1961;15:260.
[17] Manna SS, Herrmann HJ. Intermittent granular flow and clogging with internal avalanches. Eur Phys J E 2000;1:341.
[18] Zuriguel I, Pugnaloni LA, Garcimartin A, Maza D. Jamming during the discharge of grains from a silo described as a percolating transition. Phys Rev E 2003;68:030301.
[19] Valdes JR, Santamarina JC. Particle clogging in radial flow: Microscale mechanisms. Soc Pet Eng J 2006;11:193.
[20] N. Roussel TLHN, Coussot P. General probabilistic approach to the filtration process. Phys Rev Lett 2007;98:114502.
[21] D. Chen KWD, Weeks ER. Topological rearrangements and stress fluctuations in quasi-two-dimensional hopper flow of emulsions. Soft Matter 2012;8:10486.
[22] Haw MD. Jamming, two-fluid behavior, and self-filtration in concentrated particulate suspensions. Phys Rev Lett 2004;92:185506.
[23] Genovese D, Sprakel J. Crystallization and intermittent dynamics in constricted microfluidic flows of dense suspensions. Soft Matter 2011;7:3889.
[24] Aral BK, Kalyon DM. Viscoelastic material functions of noncolloidal suspensions with spherical particles. J Rheol 1997;41(3):599–620.
[25] Dersoir B, de Saint Vincent MR, Abkarian M, Tabuteau H. Clogging of a single pore by colloidal particles. Microfluid Nanofluid 2015;19(4):953–61.
[26] Toplak T, Tabuteau H, de Bruyn JR, Coussot P. Gravity draining of a yield-stress fluid through an orifice. Chem Eng Sci 2007;62(23):6908–13.
[27] Reichhardt CJO, Reichhardt C. Commensurability, jamming, and dynamics for vortices in funnel geometries. Phys Rev B 2010;81:224516.
[28] Kerner BS, Rehborn H. Experimental properties of complexity in traffic flow. Phys Rev E 1996;53:R4275.
[29] Helbing D, Farkas I, Vicsek T. Simulating dynamical features of escape panic. Nature 2000;407:487.
[30] Kondic L. Simulations of two dimensional hopper flow. Granul Matter 2014;16:235.
[31] Zuriguel I, Janda A, Garcimartín A, Lozano C, Arévalo R, Maza D. Silo clogging reduction by the presence of an obstacle. Phys Rev Lett 2011;107:278001.
[32] Thomas CC, Durian DJ. Fraction of clogging configurations sampled by granular hopper flow. Phys Rev Lett 2015;114:178001.
[33] Zuriguel I. Invited review: Clogging of granular materials in bottlenecks. Pap Phys 2014;6:060014.
[34] Tien C. Granular filtration of aerosols and hydrosols. Boston: Butterworths; 1989.
[35] Filtration and drainage in geotechnical/geoenvironmental engineering, ASCE special publication. Reston: American Society of Civil Engineers; 1998.
[36] Faure YH, Baudoin A, Pierson P, Plé O. A contribution for predicting geotextile clogging during filtration of suspended solids. Geotextile Geomembr 2006;24:11.
[37] Altoe JE, Bedrikovetsky P, Siqueira AG, de Souza ALS, Shecaira FS. Correction of basic equations for deep bed filtration with dispersion. J Pet Sci Eng 2006;51:68.
[38] Knowles P, Dotro G, Nivala J, García J. Clogging in subsurface-flow treatment wetlands: Occurrence and contributing factors. Ecol Eng 2011;37:99.
[39] Shan X, Chen H. Lattice Boltzmann model for simulating flows with multiple phases and components. Phys Rev E 1993;47(3):1815.
[40] Shan X, Chen H. Simulation of nonideal gases and liquid-gas phase transitions by the lattice Boltzmann equation. Phys Rev E 1994;49(4):2941.
[41] Higuera FJ, Succi S, Benzi R. Lattice gas dynamics with enhanced collisions. Europhys Lett 1989;9(4):345.
[42] Higuera FJ, Jimenez J. Boltzmann approach to lattice gas simulations. Europhys Lett 1989;9(7):663.
[43] Qian YH, d'Humières D, Lallemand P. Lattice BGK models for Navier–Stokes equation. Europhys Lett 1992;17(6):479.
[44] Benzi R, Succi S, Vergassola M. The lattice Boltzmann equation: Theory and applications. Phys Rep 1992;222(3):145–97.
[45] Fei L, Scagliarini A, Montessori A, Lauricella M, Succi S, Luo KH. Mesoscopic model for soft flowing systems with tunable viscosity ratio. Phys Rev Fluids 2018;3:104304.
[46] Benzi R, Chibbaro S, Succi S. Mesoscopic lattice Boltzmann modeling of flowing soft systems. Phys Rev Lett 2009;102(2):026002.
[47] Sbragaglia M, Benzi R, Bernaschi M, Succi S. The emergence of supramolecular forces from lattice kinetic models of non-ideal fluids: Applications to the rheology of soft glassy materials. Soft Matter 2012;8(41):10773–82.
[48] Benzi R, Sbragaglia M, Scagliarini A, Perlekar P, Bernaschi M, Succi S, et al. Internal dynamics and activated processes in soft-glassy materials. Soft Matter 2015;11(7):1271–80.
[49] Dollet B, Scagliarini A, Sbragaglia M. Two-dimensional plastic flow of foams and emulsions in a channel: Experiments and lattice Boltzmann simulations. J Fluid Mech 2015;766:556–89.
[50] Succi S. The lattice Boltzmann equation: For fluid dynamics and beyond. Oxford University Press; 2001.
[51] Succi S. The lattice Boltzmann equation: For complex states of flowing matter. Oxford University Press; 2018.
[52] Bullard JW, Pauli AT, Garboczi EJ, Martys NS. A comparison of viscosity–concentration relationships for emulsions. J Colloid Interface Sci 2009;330(1):186–93.
[53] Wilson TJ, Pfeifer CR, Mesyngier N, Durian DJ. Granular discharge rate for submerged hoppers. 2013, arXiv preprint arXiv:1307.2812.
[54] Koivisto J, Durian DJ. Effect of interstitial fluid on the fraction of flow microstates that precede clogging in granular hoppers. Phys Rev E 2017;95(3):032904.
[55] Sheng JJ. Enhanced oil recovery field case studies. Gulf Professional Publishing; 2013.
[56] Fei L, Scagliarini A, Luo KH, Succi S. Discrete fluidization of dense monodisperse emulsions in neutral wetting microchannels. Soft Matter 2020;16(3):651–8.